Journal of Materials Chemistry B

RSC Publishing

PAPER

View Article Online
View Journal | View Issue

Cite this: J. Mater. Chem. B, 2013, 1, 4160

Microwave-assisted synthesis of highly luminescent $AgInS_2$/ZnS nanocrystals for dynamic intracellular Cu(II) detection†

Wei-Wei Xiong, Guo-Hai Yang, Xing-Cai Wu* and Jun-Jie Zhu*

Received 2nd May 2013
Accepted 24th June 2013

DOI: 10.1039/c3tb20638f

www.rsc.org/MaterialsB

Low-toxicity, highly luminescent, and water-soluble $AgInS_2$/ZnS nanocrystals (NCs) have been synthesized *via* a microwave-assisted approach. The structure and optical features of the $AgInS_2$/ZnS NCs were characterized by X-ray diffraction, high resolution transmission electron microscopy, Fourier transform infrared spectroscopy, ultraviolet visible absorption spectroscopy and photoluminescence (PL) spectroscopy. The as-synthesized $AgInS_2$/ZnS NCs exhibited high PL quantum yields (40%) and long PL lifetimes (424.5 ns). Furthermore, the dynamic changes of the intracellular copper(II) levels in HeLa cells were monitored using the $AgInS_2$/ZnS NCs as fluorescent probes. The results showed that the $AgInS_2$/ZnS NCs as promising fluorescent probes can be used in the detection of intracellular copper ions in living cells.

1 Introduction

In recent decades, quantum dots (QDs) have experienced rapid development. In particular, II–VI Cd-based QDs have been widely applied in solar cells, LEDs, sensors and biomedical imaging.[1–4] However, the applications of the Cd-based QDs have been limited due to the toxicity of Cd, which leads to a strong interest in the search for alternative semiconductor nanoparticles with low-toxicity heavy metal ions.[5]

Recent research has shown that the I–III–VI ternary semiconductor nanoparticles such as $AgInS_2$ and $CuInS_2$ are promising candidates, because of their direct bandgaps, large absorption coefficients, long photoluminescence (PL) lifetimes and low toxicity.[6–11] Several methods have been reported for the synthesis of $AgInS_2$ nanoparticles such as hot injection,[6–8] solvothermal,[13] single-source precursor,[14,15] thermolysis and hydrothermal methods.[16] However, they were mostly carried out in organic solvents, and some of the complex precursors were necessary, and it may be difficult for them to be applied in biology due to their hydrophobic properties. The process of phase transfer from the organic to aqueous solution is also relatively complicated and often associated with the significant decrease of both the PL quantum yields (QYs) and stability. Compared to the organic solvent synthesis, the aqueous phase synthesis of nanoparticles is simpler, cheaper and more biocompatible.[17] However, in the case of ternary nanoparticles, only a few references report the synthesis in aqueous solution.[18,19]

Microwave irradiation is an attractive method for the synthesis of nanoparticles, which has unique characteristics such as rapid and uniform heating to shorten the reaction time.[20,21] In addition, intracellular Cu^{2+} ions play a critical role in physiological and pathological events, for example, the dysfunction of copper metabolism has been suggested in many diseases such as Menkes disease, Wilson disease, and some neurodegenerative diseases.[22–25] Hence, it is important to monitor intracellular Cu^{2+} concentration in living cell.

Herein, a novel microwave irradiation approach was used for the fast synthesis of water-soluble $AgInS_2$/ZnS NCs. The PL QYs of the $AgInS_2$/ZnS NCs were up to 40%, which was reasonably good as compared with some of the previously reported product *via* organic synthetic procedures.[7,26] At the meantime, the high fluorescence $AgInS_2$/ZnS NCs has good selectivity and sensitivity for copper ions, which can be used as probes to detect intracellular Cu^{2+}. Therefore, a new strategy was developed to detect intracellular Cu^{2+} in living cells using the $AgInS_2$/ZnS NCs as fluorescent probes.

2 Experimental section

2.1 Materials

Indium nitrate hydrate ($In(NO_3)_3 \cdot 4H_2O$, 99.9%), and reduced glutathione (GSH, 99%) were purchased from Aladdin Chemistry Co. Ltd (China). Silver nitrate ($AgNO_3$, 99.8%), zinc acetate dehydrate ($Zn(Ac)_2 \cdot 2H_2O$, 98%), and sodium sulfide (Na_2S, 99%), were purchased from Nanjing chemical reagent Co. Ltd (China). Rhodamine 6G (99%) was obtained from Sigma-Aldrich. All other reagents were of analytical reagent grade. All aqueous solutions were prepared using ultrapure water (Milli-Q, Millipore).

State Key Lab. of Analytical Chemistry for Life Science, Key Lab. of Mesoscopic Chemistry of MOE, School of Chemistry and Chemical Engineering, Nanjing University, Nanjing, 210093, P. R. China. E-mail: wuxingca@nju.edu.cn; jjzhu@nju.edu.cn; Fax: +86-25-83597204; Tel: +86-25-83597204

† Electronic supplementary information (ESI) available. See DOI: 10.1039/c3tb20638f

2.2 Microwave-assisted synthesis of $AgInS_2$/ZnS NCs

First, $AgInS_2$ NCs were synthesized in aqueous solution *via* a microwave irradiation approach. In a typical experiment, 0.1 mL $AgNO_3$ (0.1 M) and 0.4 mL $In(NO_3)_3$ (0.1 M) solution were added in 18.4 mL distilled water, followed by the addition of 1.6 mL of 0.1 M GSH. pH of the solution was then adjusted to 8.5 by the addition of 1.0 M NaOH solution. During this process, the solution changed from turbid to clear. After that, 0.8 mL of freshly prepared Na_2S solution (0.05 M) was added into the mixture solution. 20 mL of the $AgInS_2$ precursor was then injected into the exclusive vitreous vessel with a volume of 80 mL. High-quality $AgInS_2$ NCs were prepared at controlled reaction temperature of 100 °C. After microwave irradiation for 5 min, the mixture was allowed to cool to lower than 50 °C and the $AgInS_2$ NCs were separated and purified *via* ultrafiltration with a Microncon YM-30 kDa filtration device.

Then, 0.8 mL of 0.1 M $Zn(Ac)_2$ and 0.8 mL of 0.05 M Na_2S solution were injected into the $AgInS_2$ NCs for the preparation of the $AgInS_2$/ZnS NCs. The mixture was further irradiated at 100 °C for 5 min, followed by purification using ultrafiltration.

2.3 Cell culture and MTT assay

HeLa cells were cultured in Dulbecco's Modified Eagle's medium (DMEM) containing high glucose supplemented with 10% fetal bovine serum, 100 units mL^{-1} Penicillin and 100 μg mL^{-1} streptomycin. At the logarithmic growth phase, HeLa cells ($\sim 5 \times 10^5$ cells per mL) were placed at a 96-well plate, incubated at 37 °C and the humidified atmosphere with 5% CO_2 for 12 h. Then, the DMEM medium was replaced by fresh DMEM medium in the presence of different concentrations of $AgInS_2$/ZnS NCs, and the cells were further incubated for 24 h. Then, 100 μL of the culture media containing MTT (10 μL, 5 mg mL^{-1}) was added, followed by incubating for 4 h to allow the formation of formazan dye. The medium was then removed, and 110 μL of dimethyl sulfoxide (DMSO) was added to dissolve the purple formazan crystals, followed by 10 min incubation. Absorbance was measured at 490 nm in a Bio-rad 680 microplate photometer. The relative cell viability was defined as $(A_{test}/A_{blank}) \times 100\%$, where A is absorbance.

2.4 Cell imaging

Fluorescent images of the cells were taken by Leica TCS SP5 inverted confocal microscope (CLSM) equipped with a 63 × 1.32 NA oil immersion objective. Before imaging, cells were placed on a 35 mm Petri dish with 15 mm bottom well in the DMEM medium with 10% fetal bovine plasma in 5% CO_2 at 37 °C overnight to get a suitable density. Then the medium was replaced by a fresh serum-free medium containing 0.02 mg mL^{-1} $AgInS_2$/ZnS NCs and incubated for 2 h. After that, the cells were washed three times with PBS and incubated with DMEM containing 10% fetal bovine plasma for additional 4 h. Finally, the cells were collected and washed three times with PBS before imaging. For cellular copper ion imaging, a certain concentration of copper ion solution was further added to the Petri dish.

2.5 Characterization

The ultraviolet-visible (UV-Vis) absorption spectra were obtained using a UV-3600 spectrophotometer (Shimadzu, Japan). The PL measurements were carried out using a Bruker RF-5301PC fluorescence spectrometer. High-resolution transmission electron microscopy (HRTEM) images were taken using a JEOL2010 electron microscope at an acceleration voltage of 200 KV. XRD patterns were obtained using XRD-6000 diffraction with Cu Kα radiation. Fourier transform infrared (FTIR) were recorded with a Bruker Vector 22 FTIR spectrometer. The PL lifetimes study was performed by FLS920 (Edinburgh Instruments) with excitation at 409 nm. The microwave system is from Discover (CEM, America), and exclusive vitreous vessels with 80 mL is equipped for the system with high temperature and pressure.

3 Results and discussion

3.1 Characterization

The crystal structure of the NCs was analyzed by XRD. Fig. 1a shows the XRD patterns of the $AgInS_2$ NCs and $AgInS_2$/ZnS NCs with significant line broadening with respect to those of the bulk counterparts. The broadening diffraction peaks suggests small sizes of $AgInS_2$ NCs and $AgInS_2$/ZnS NCs. The XRD pattern of $AgInS_2$ NCs consists of three major peaks at 2θ values of 26.9°, 45.0°, and 52.3°, corresponding to the (112), (204) and (312) indices of $AgInS_2$ with the tetragonal structure (JCPDS No. 75-0117), respectively. Similar features were observed for the $AgInS_2$/ZnS NCs, but the corresponding peaks were slightly right-shifted with respect to the $AgInS_2$ NCs, indicating that Zn^{2+} diffusion results in change of the lattice parameters of the $AgInS_2$/ZnS NCs.[12] The EDS of the $AgInS_2$/ZnS NCs clearly showed the presence of Ag, In, Zn, and S (Fig. S1, ESI†).

The morphologies, sizes, and structures were further characterized by HRTEM images. As shown in Fig. 1b, the monodispersed $AgInS_2$ NCs have average sizes of about 2.5 nm, and the fringe space of 0.32 nm corresponds to the *d*-value of the

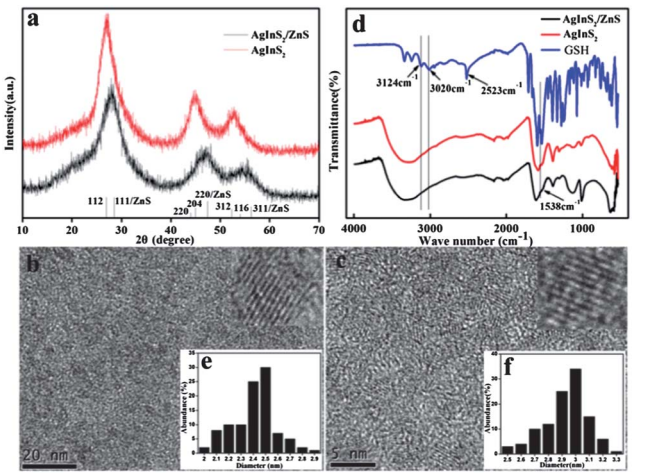

Fig. 1 (a) X-ray diffraction patterns of $AgInS_2$ NCs and $AgInS_2$/ZnS NCs. (b and c) HRTEM images of the $AgInS_2$ NCs and $AgInS_2$/ZnS NCs (Inset e and f: histogram showing the size distribution of the NCs). (d) FTIR spectra of glutathione, $AgInS_2$ NCs and $AgInS_2$/ZnS NCs.

(112) index of the tetragonal $AgInS_2$. While the average size of the resulting $AgInS_2$/ZnS NCs increases to 3.0 nm as shown in Fig. 1c, which is slightly bigger than that of the $AgInS_2$ NCs.

To verify the existence of GSH on the surface of the nanocrystals as a stabilizer, we compared the FTIR spectra of free GSH and GSH-capped NCs. As shown in Fig. 1d, the FTIR absorption bands of free GSH at 3124 cm^{-1} and 3020 cm^{-1} are ascribed to N–H stretching bands (NH_3^+), whereas the peak at 2523 cm^{-1} and 1538 cm^{-1} are assigned to –SH and –NHR groups, respectively. In contrast, the disappearance of the –SH stretching vibrational peak, the almost disappearance of the N–H stretching bands, and the weakening of the amide bond clearly indicates that GSH may be combined into the surface of the NCs through the –SH and –NHR groups.

3.2 UV-Vis absorption and PL spectra

Fig. 2 shows the UV-Vis absorption and the PL spectra of the NCs. The UV-Vis absorption edges of $AgInS_2$ NCs and $AgInS_2$/ZnS NCs were 426 nm (2.66 eV) and 466 nm (2.91 eV), respectively. Compared to the $AgInS_2$ NCs, the absorption spectra of the $AgInS_2$/ZnS NCs shift to high energy, which comes from the alloy structure of ZnS (band gap of 3.7 eV).[26]

The dashed lines in Fig. 2 show the PL excitation (PLE) and emission spectra. The PL spectra showed a broad, nearly Gaussian emission band. The peak position and full width at half-maximum (FWHM) of the $AgInS_2$ NCs were 570 nm and 68 nm at excitation of 470 nm, respectively, while those of the $AgInS_2$/ZnS NCs were 553 nm and 82 nm at excitation of 453 nm, respectively. The PL emission peak of the $AgInS_2$/ZnS NCs shows a blue shift in comparison with $AgInS_2$ NCs. Both stokes shifts were 100 nm. The quantum yields of the $AgInS_2$ NCs and $AgInS_2$/ZnS NCs were 14% and 40%, respectively. The photographs of water-soluble $AgInS_2$ NCs and $AgInS_2$/ZnS NCs under a 365 nm UV illumination are shown in Fig. S2† (ESI).

3.3 Influence of experiment variables on the PL properties of $AgInS_2$ NCs and $AgInS_2$/ZnS NCs

In order to optimize the PL properties of $AgInS_2$ NCs, we investigated the ratios of Ag/In, In/GSH, In/S and pH value on the effect of the PL intensity. We changed one experimental variable,

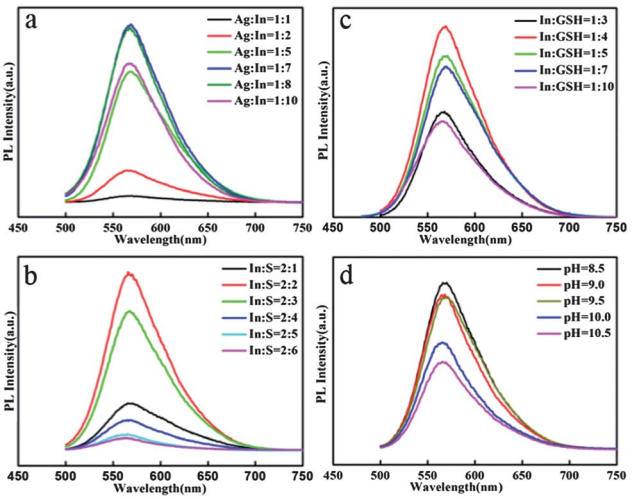

Fig. 3 The effect of the ratios of Ag : In, In : GSH, In : S and pH value on the PL intensity.

and kept the other variables constant. Fig. 3a shows the PL intensity of $AgInS_2$ NCs while the ratio of Ag/In was changed from 1 : 1 to 1 : 10. In the curves, the PL intensity of the $AgInS_2$ NCs increased gradually with the decreasing Ag content. The PL intensity reached the maximum value at the ratio of 1 : 7, following gradually decreased PL intensity. To investigate the influence of the molar ratios of In: S on the PL intensity, the amount of Na_2S to obtain the ratios was changed from 2 : 1 to 2 : 6. The PL intensity reached to the maximum as shown in Fig. 3b when the In : S was 1. A commonly accepted transition mechanism is donor–acceptor pair (DA) recombination, where In_{Ag} (In substituted at the Ag site) and/or V_S (S vacancy) are likely to act as donor states with V_{Ag} (Ag vacancy) as an acceptor state.[13,27] An alternative carrier recombination between the quantized conduction band minimum and defect (acceptor) trap level is also persuasive as proposed by Nose *et al.*[28] The amount of Ag vacancies has been reported to play an important role in the enhancement of PL intensity, and the PL intensity increased with Ag/In ratios.[14] On the one hand, the appropriate In : Ag and In : S ratios can help carrier recombination, enhancing the PL emission. On the other hand, when the In : Ag and In : S ratios were

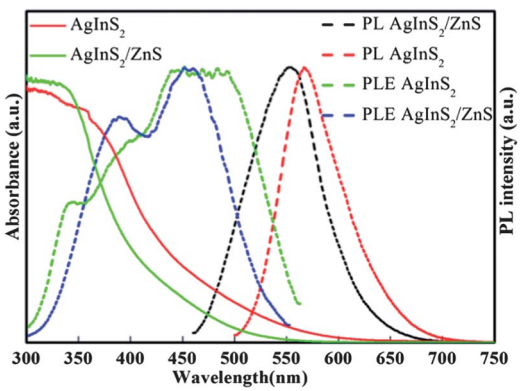

Fig. 2 UV-Vis, PLE and PL spectra of the $AgInS_2$ NCs and $AgInS_2$/ZnS NCs.

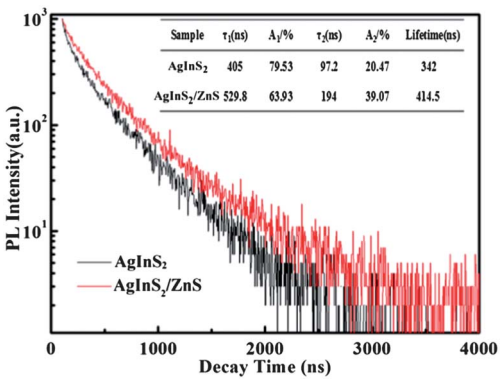

Fig. 4 PL decays curves of $AgInS_2$ NCs and $AgInS_2$/ZnS NCs.

large enough, the concentration of recombination center increased dramatically thus suppressing the PL emission.

Fig. 3c shows the relative PL intensity of the $AgInS_2$ NCs with In : GSH molar ratios ranging from 1 : 3 to 1 : 10. The sample with an In : GSH molar ratios of 1 : 4 showed the strongest PL emission. It is known that the surface defects provide sites for charge trapping to induce non-radiative recombination of electrons and holes, resulting in quenching of photoluminescence. Therefore, appropriate concentration of GSH can reduce surface defects to enhance PL emission, whereas excessive GSH might distort the surface, and weaken the PL emission.

pH value also has a large effect on the PL intensity of $AgInS_2$ NCs, as shown in Fig. 3d. The pH value changed from 8.5 to 10.5. When the pH value was below 8.5, the solution turned turbid. With the increasing pH value, the PL intensity of the $AgInS_2$ NCs decreased gradually. The reason was probably that the GSH pK_a value is 8.7, and between the GSH and $AgInS_2$ NCs show stronger bonding forces at this pH value.[18]

To further improve the PL intensity of the $AgInS_2$ NCs, ZnS was chosen to modify $AgInS_2$ NCs. Because of the effective surface passivation by the ZnS overlayer, the PL intensity of the $AgInS_2$/ZnS NCs was dramatically increased, and the highest PL QYs reached 40%.

3.4 PL lifetimes

Fig. 4 shows the PL decay curves of $AgInS_2$ NCs and $AgInS_2$/ZnS NCs with the emission peaks at 570 and 540 nm, and the corresponding average PL lifetime values were 342 and 414.5 ns, respectively. The decay curves were multi-exponential in nature and excited at 409 nm. The decay curves were well fitted by the following equation form:

$$I(t) = A1\exp\left(-\frac{t}{\tau_1}\right) + A2\exp\left(-\frac{t}{\tau_2}\right)$$

where τ_1 and τ_2 represent the decay time of the PL mission and $A1, A2$ represent the relative weights of the decay components at $t = 0$.[29] Based on the obtained lifetime values, we attribute the fast decay time component to the radiative recombination processes of the surface defect states, whereas the slower decay times are due to the radiative recombination processes of the donor–acceptor pairs or deep defect-related recombination mechanism. Surface-related trap states are usually shallow and therefore show faster decay lifetime than the intrinsic defect-related trap states.[30] Compared to the Cd-based QDs, the NCs have longer PL lifetimes and lower toxicity, so that they are more suitable for biological imaging.

3.5 Cytotoxicity assay (MTT) and detection of intracellular copper ions

For biological applications, MTT assays were carried out to evaluate the cytotoxicity of $AgInS_2$/ZnS NCs to HeLa cells. As expected, the viability of the HeLa cells only declined by <10% upon addition of the $AgInS_2$/ZnS NCs up to 0.20 mg mL^{-1} (Fig. S3, ESI†). Thus, the $AgInS_2$/ZnS NCs probes can be considered to have low toxicity and be biocompatible for the detection of Cu^{2+} ions in living cells.

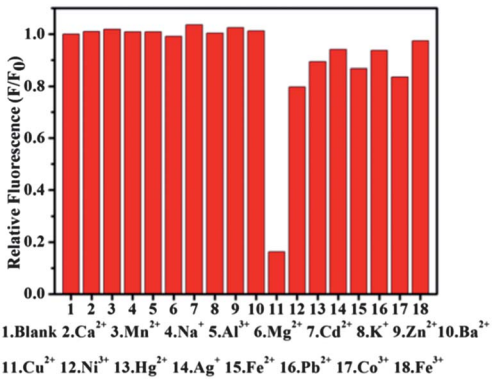

Fig. 5 Fluorescence responses of $AgInS_2$/ZnS NCs (0.02 mg mL^{-1}) towards various cations ions (1 mM for Na^+, K^+, Ca^{2+} and Mg^{2+}; 10 μM for others cations).

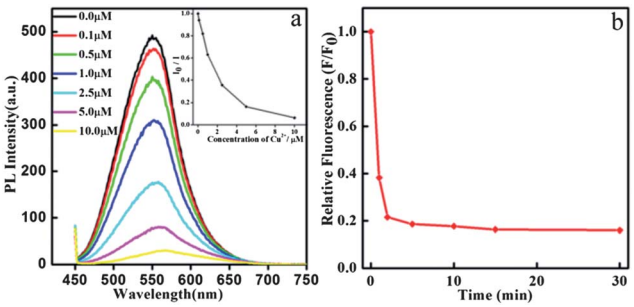

Fig. 6 (a) Fluorescence spectra of $AgInS_2$/ZnS NCs (0.02 mg mL^{-1}) exposed to different amounts of Cu^{2+}. (Inset: the correlation curve of I_0/I as a function of the concentration of Cu^{2+} from 0.1 μM to 10 μM). (b) Time-dependent fluorescence response of the $AgInS_2$/ZnS NCs (0.02 mg mL^{-1}) probes to Cu^{2+} (10 μM).

To evaluate the selectivity, the PL quenching effect of 17 kinds of cations to the $AgInS_2$/ZnS NCs probes was investigated. As shown in Fig. 5, only a small change in the PL intensity was observed for the cation ions except Cu^{2+} ions, showing that the probes have high selectivity for Cu^{2+} ions. The phenomena can be explained in terms of strong binding of Cu^{2+} onto the surface of $AgInS_2$/ZnS NCs leading to a chemical displacement of Zn^{2+}

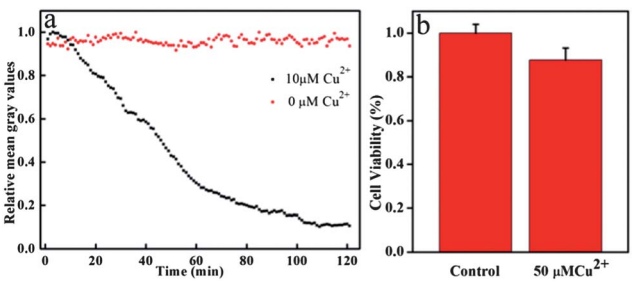

Fig. 7 (a) Relative mean gray values–time curves in the intracellular of the HeLa cells with and without treatment with 10 μM Cu^{2+} in 10 mM PBS. The HeLa cells was first incubated with $AgInS_2$/ZnS NCs (0.02 mg mL^{-1}). (b) Cell viability Assay of HeLa cells treated with the exogenous Cu source (50 μM Cu^{2+} in PBS) for 2 h. The HeLa cells was first incubated with $AgInS_2$/ZnS NCs (0.02 mg mL^{-1}) in fresh serum-free medium for 2 h, and then incubated with a fresh serum-containing medium for 4 h.

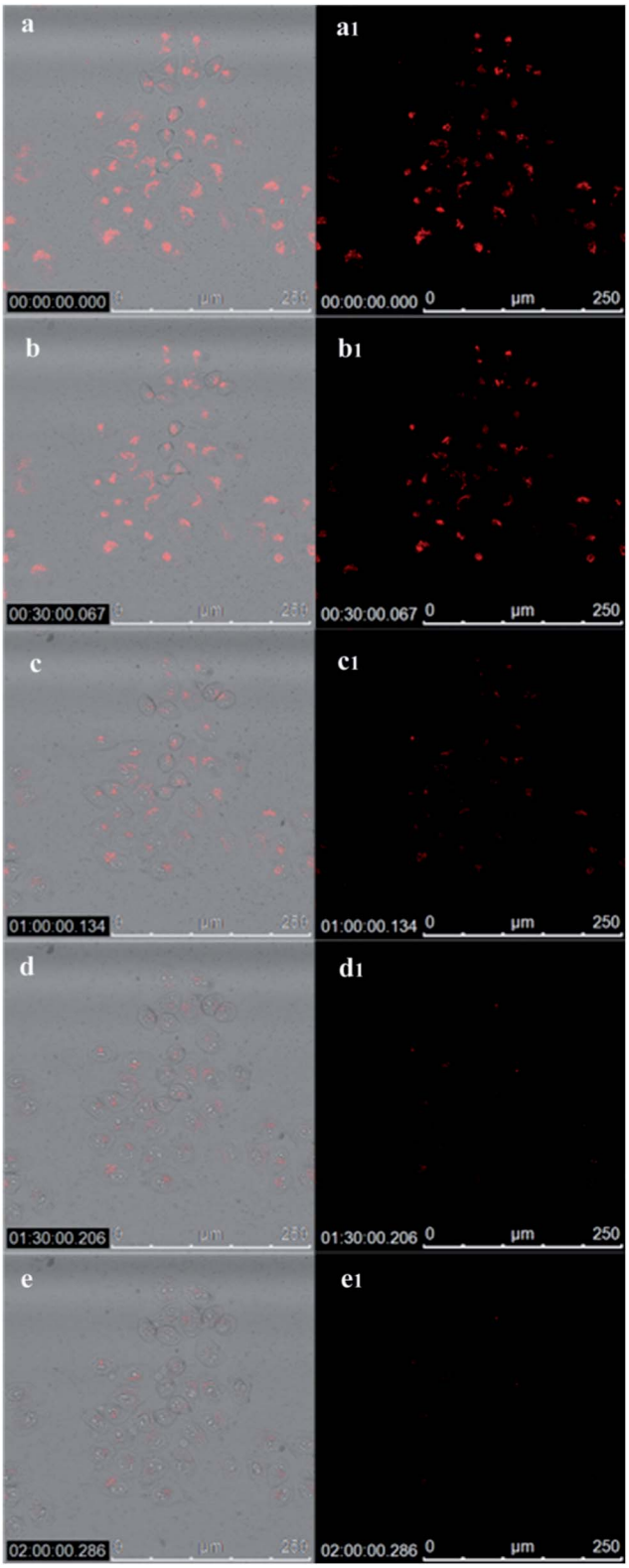

Fig. 8 The overlay of bright-field and fluorescence images (a–e) and their corresponding fluorescence images (a_1–e_1) of HeLa cells after adding the exogenous Cu source (10 μM Cu^{2+} in PBS) with different times (0, 30, 60, 90, and 120 min). The HeLa cells were first incubated with $AgInS_2$/ZnS NCs (0.02 mg mL^{-1}) in fresh serum-free medium for 2 h, and then incubated with a fresh serum-containing medium for 4 h before imaging.

and the subsequent formation of CuS, which quenched the fluorescence of these NCs. In the emission spectrum (see Fig. 6a), the red-shift of the NCs after the addition of Cu^{2+} was observed, indicating the formation of CuS on the surface of NCs. The formation of CuS at the surface of NCs caused quenching of the luminescence by facilitating non-radiative electron/hole annihilation.[31] The probes show good correlation curves from 0.1 μM to 10 μM as shown in Fig. 6a. In addition, the reaction between the $AgInS_2$/ZnS NCs probes and Cu^{2+} ions was quick (Fig. 6b). This observation suggested that the $AgInS_2$/ZnS NCs were sensitive to Cu^{2+} ions, and could be employed as fluorescent probes for real-time monitoring of Cu^{2+} ions in biological systems. In addition, Cu(II) ions are known to produce reactive oxygen species (ROS) in intracellular environment.[32] In order to rule out the possibility of ROS quenching fluorescence of the probes, we assess the effect of ROS on the PL intensity of $AgInS_2$/ZnS probes as shown in Fig. S4 (ESI†). Therefore, the effect of ROS could be precluded.

To explore the feasibility of the $AgInS_2$/ZnS NCs probes in intracellular Cu^{2+} imaging. A quantitative program of CLSM was used to monitor the dynamic changes in the intracellular copper(II) levels in HeLa cells. In the experiment, HeLa cells were first incubated with DMEM containing $AgInS_2$/ZnS NCs probes for 2 h. After that, the cells were washed three times with PBS and incubated with DMEM containing 10% fetal bovine plasma for additional 4 h to enhance the cell viability. Then, 10 μM Cu $(NO_3)_2$ was employed to increase the intracellular level of the Cu^{2+} ions. As shown in Fig. 7a, the intracellular relative fluorescence intensity decreased gradually with time. The changes were attributed to the continuous fluorescence quenching by intracellular Cu^{2+} ions, which was consistent with the change of the fluorescence spectrum in Fig. 6a. In addition, no obvious changes of the fluorescence intensity were observed in the absence of copper ions, indicating that $AgInS_2$/ZnS NCs has good stability and resistance to bleaching. CLSM was also used to visualize the fluorescence quenching process inside HeLa cells. As shown in Fig. 8, the pictures display the fluorescence images with different time (0, 30, 60, 90 and 120 min). The intracellular fluorescence from the probes were almost completely suppressed after incubation with 10 μM Cu^{2+} for 2 h. Besides, cell viability measurements after treatment with $AgInS_2$/ZnS NCs probes and Cu^{2+} (50 μM) confirmed that the cells were viable throughout the imaging (Fig. 7b). These results indicated that $AgInS_2$/ZnS NCs were an effective intracellular Cu^{2+} imaging probe for the biological applications.

4 Conclusion

In this work, the water-soluble highly fluorescent $AgInS_2$/ZnS NCs were fabricated by a microwave-assisted method. Compared with the traditional synthesis in an organic solvent, the proposed method is simpler, cheaper and more biocompatible. The as-prepared NCs showed high fluorescence, low toxicity and long PL lifetimes. Furthermore, the $AgInS_2$/ZnS NCs were applied to detect intracellular copper ions, showing that it was promising as a fluorescent probe in biological and biomedical imaging.

Acknowledgements

We greatly appreciate the financial support from National Natural Science Foundation of China (NSFC) (nos 21121091, 21171091) and the support from 973 Program (no. 2011CB933502).

Notes and references

1 M. Shalom, S. Ruhle, I. Hod, S. Yahav and A. Zaban, *J. Am. Chem. Soc.*, 2009, **131**, 9876.
2 I. L. Medintz, A. R. Clapp, H. Mattoussi, E. R. Goldman, B. Fisher and J. M. Mauro, *Nat. Mater.*, 2003, **2**, 630.
3 P. Zrazhevskiy, M. Sena and X. H. Gao, *Chem. Soc. Rev.*, 2010, **39**, 4326.
4 Y. Y. Shen, L. L. Li, Q. Lu, J. Ji, R. Fei, J. R. Zhang, E. S. Abdel-Halim and J. J. Zhu, *Chem. Commun.*, 2012, **48**, 2222.
5 K. M. Tsoi, Q. Dai, B. A. Alman and W. C. W. Chan, *Acc. Chem. Res.*, 2013, **46**, 662.
6 P. M. Allen and M. G. Bawendi, *J. Am. Chem. Soc.*, 2008, **130**, 9240.
7 R. G. Xie, M. Rutherford and X. G. Peng, *J. Am. Chem. Soc.*, 2009, **131**, 5691.
8 J. Park and S. W. Kim, *J. Mater. Chem.*, 2011, **21**, 3745.
9 J. Y. Chang, G. Q. Wang, C. Y. Cheng, W. X. Lin and J. C. Hsu, *J. Mater. Chem.*, 2012, **22**, 10609.
10 B. K. Chen, H. Z. Zhong and B. S. Zou, *Prog. Chem.*, 2011, **23**, 2276.
11 X. Yuan, J. L. Zhao, P. T. Jing, W. J. Zhang, H. B. Li, L. G. Zhang, X. H. Zhong and Y. Masumoto, *J. Phys. Chem. C*, 2012, **116**, 11973.
12 X. S. Tang, W. B. A. Ho and J. M. Xue, *J. Phys. Chem. C*, 2012, **116**, 9769.
13 D. E. Nam, W. S. Song and H. Yang, *J. Mater. Chem.*, 2011, **21**, 18220.
14 M. L. Dai, S. Ogawa, T. Kameyama, K. Okazaki, A. Kudo, S. Kuwabata, Y. Tsuboi and T. Torimoto, *J. Mater. Chem.*, 2012, **22**, 12851.
15 M. L. Dai, K. Okazaki, A. Kudo, S. Kuwabata and T. Torimoto, *Electrochemistry*, 2011, **79**, 790.
16 S. Y. Liu, H. Zhang, Y. Qiao and X. G. Su, *RSC Adv.*, 2012, **2**, 819.
17 Y. Y. Su, Y. He, H. T. Lu, L. M. Sai, Q. N. Li, W. X. Li, L. H. Wang, P. P. Shen, Q. Huang and C. H. Fan, *Biomaterials*, 2009, **30**, 19.
18 Z. S. Luo, H. Zhang, J. Huang and X. H. Zhong, *J. Colloid Interface Sci.*, 2012, **377**, 27.
19 Y. G. Zheng, M. Y. Han, M. D. C. Regulacio, S. Y. Zhang, X. H. Zhang, K. Y. Win and S. Wang, *Nanoscale*, 2013, **5**, 2322.
20 H. F. Qian, X. Qiu, L. Li and J. C. Ren, *J. Phys. Chem. B*, 2006, **110**, 13352.
21 H. J. Zhan, P. J. Zhou, Z. Y. He and Y. Tian, *Eur. J. Inorg. Chem.*, 2012, 2487.
22 E. L. Que, E. J. New and C. J. Chang, *Chem. Sci.*, 2012, **3**, 1829.
23 J. Liu and Y. Lu, *J. Am. Chem. Soc.*, 2007, **129**, 9838.
24 A. W. Zhu, Q. Qu, X. L. Shao, B. Kong and Y. Tian, *Angew. Chem., Int. Ed.*, 2012, **51**, 7185.
25 T. Y. Cheng, Y. F. Xu, S. Y. Zhang, W. P. Zhu, X. H. Qian and L. P. Duan, *J. Am. Chem. Soc.*, 2008, **130**, 16160.
26 (*a*) B. D. Mao, C. H. Chuang, J. W. Wang and C. Burda, *J. Phys. Chem. C*, 2011, **115**, 8945; (*b*) B. D. Mao, C. H. Chuang, F. Lu, L. X. Sang, J. J. Zhu and C. Burda, *J. Phys. Chem. C*, 2013, **117**, 648.
27 W. S. Song and H. Yang, *Chem. Mater.*, 2012, **24**, 1961.
28 K. Nose, Y. Soma, T. Omata and S. O. Y. Matsuo, *Chem. Mater.*, 2009, **21**, 2607.
29 L. Li, A. Pandey, D. J. Werder, B. P. Khanal, J. M. Pietryga and V. I. Klimov, *J. Am. Chem. Soc.*, 2011, **133**, 1176.
30 V. K. Komarala, C. Xie, Y. Q. Wang, J. Xu and M. Xiao, *J. Appl. Phys.*, 2012, **111**, 124314.
31 H. Y. Xie, H. G. Liang, Z. L. Zhang, Y. Liu, Z. K. He and D. W. Pang, *Spectrochim. Acta, Part A*, 2004, **60**, 2527.
32 L. M. Gaetke and C. K. Chow, *Toxicology*, 2003, **189**, 147.